Interplay of Kitaev Interaction and Off-Diagonal Exchanges: Exotic Phases and Quantum Phase Diagrams

Qiang Luo(罗强)[1,2*], Jize Zhao(赵继泽)[3,4], and Xiaoqun Wang(王孝群)[5*]

[1]*College of Physics, Nanjing University of Aeronautics and Astronautics, Nanjing 211106, China*
[2]*Key Laboratory of Aerospace Information Materials and Physics (NUAA), MIIT, Nanjing 211106, China*
[3]*School of Physical Science and Technology & Key Laboratory of Quantum Theory and Applications of MoE, Lanzhou University, Lanzhou 730000, China*
[4]*Lanzhou Center for Theoretical Physics, Key Laboratory of Theoretical Physics of Gansu Province, Lanzhou University, Lanzhou 730000, China*
[5]*School of Physics and Institute for Advanced Study in Physics, Zhejiang University, Hangzhou 310058, China*

(Received 18 November 2024; accepted manuscript online 24 December 2024)

Aligning with the ongoing search for quantum spin liquids (QSLs), identifying QSLs in Kitaev magnets has attracted significant research interest during the past decade. Nevertheless, it remains a significant challenge. One of the major difficulties is that Kitaev QSL is typically fragile to competing interactions such as off-diagonal exchanges, which are ubiquitous in real materials owing to spin-orbit coupling and crystal-field effects. This, in turn, generates many intriguing field-induced novel phases and the thermal Hall effect. In this review, we focus on the interplay between the Kitaev interaction and off-diagonal Γ and Γ' exchange from a numerical perspective. The review discusses certain representative exotic phases such as Γ spin liquid, nematic ferromagnet, spin-flop phase, and distinct chiral spin states with spontaneous time-reversal symmetry breaking. It also presents quantum phase diagrams of anisotropic Kitaev-Γ chains that exhibit kaleidoscopy for both ordered and disordered phases.

DOI: 10.1088/0256-307X/42/2/027501 CSTR: 32039.14.0256-307X.42.2.027501

1. Introduction. The experimental search for and theoretical prediction of exotic states of matter such as quantum spin liquids (QSLs) remain significant challenges in advanced condensed matter research.[1–4] Initiated by Anderson over half a century ago,[5] the concept of QSL has attracted significant attention. This is because it extends beyond Landau's paradigm, which characterizes phases by spontaneous symmetry breaking and local order parameters. The QSL is a highly entangled magnetic state characterized by fractionalized excitations and a continuous spectrum. It plays a potential role in topologically protected quantum computing.[6] For many years, low-dimensional quantum magnets with geometrical frustration and/or competing interactions have been acknowledged as attractive arenas to probably harbor QSLs. The prominent examples include the Heisenberg model for the Kagome lattice[7,8] and the J_1-J_2 model on a triangular[9,10] or square lattice.[11,12]

Following Kitaev's pioneering work in 2006,[13] the introduction of the Kitaev interaction has revolutionized the research on spin-liquid physics. The spin-1/2 Kitaev honeycomb model has been demonstrated to be solvable. Its ground state is called the Kitaev QSL, which contains fractionalized Majorana fermions.[13] This solvability is vital because it provides an exhaustive understanding of the intricate behaviors exhibited by QSLs. Since then, Kitaev materials with non-negligible Kitaev interactions have been studied extensively (for reviews, see Refs. [14–17]). In the early stages of evaluating Kitaev materials, attention was focused mainly on $4d/5d$ transition-metal compounds.[18–20] Here, α-$RuCl_3$ was the most prominent material.[20] Accompanied by a deeper understanding of the microscopic mechanism of Kitaev interaction, the interest in cobaltates[21–24] and rare earth chalcohalides[25] is growing. Evidence of Kitaev interactions has also been observed in certain Ni/Cr-based van der Waals magnets, albeit with higher spins.[26–32] However, the sought-after QSL has not been achieved experimentally. This is because in real materials, the isotropic Heisenberg interactions and off-diagonal exchanges are not suppressed fully and compete with the Kitaev term. This usually results in magnetically ordered ground states such as zigzag ordering.[33]

It is noteworthy that there are many remarkable reviews pertaining to the Kitaev physics, both theoretical and experimental. Hermanns *et al.* reviewed the Kitaev honeycomb model in terms of fractionalization, dynamic correlations, and material connections.[14] Takagi *et al.* reviewed the concept and realization of Kitaev QSL in candidate materials.[15] Trebst and Hickey reviewed the status of the evaluation of representative Kitaev materials.[16] Rousochatzakis *et al.* reviewed many emergent phenomena beyond Kitaev physics.[17]

In this short review, we focus on the exotic phases and

*Corresponding author. Email: qiangluo@nuaa.edu.cn; xiaoqunwang@zju.edu.cn
© 2025 Chinese Physical Society and IOP Publishing Ltd. All rights, including for text and data mining, AI training, and similar technologies, are reserved.

quantum phase diagrams studied by us and our collaborators in the domain of the $JK\Gamma\Gamma'$ model. The main concerns of exotic phases are the gapless Γ spin liquid (ΓSL) in the honeycomb Γ model,[34] chiral spin state and nematic ferromagnets in the spin-1 Kitaev-Γ model,[35] and chiral-spin ordering and the spin-flop phase in the Γ-Γ' model.[36,37] The quantum phase diagrams of the spin-1/2 and spin-1 bond-alternating Kitaev-Γ chains are summarized.[38,39] This is followed by an evaluation of the Kitaev phase.[40] Thereby, we aim to provide insights to aid the research and advancement of unconventional quantum criticality in frustrated magnets.

2. Model and Relevant Material. In transition metal compounds with edge-sharing octahedra, the interplay of spin-orbit coupling and the crystal-field effect conspires bond-directional Ising-type interactions. This results in the formation of a large family of Kitaev materials on honeycomb lattices.[18] Although these materials have different magnetic ground states and display distinguishing magnetic-field-induced phenomena, the paradigm $JK\Gamma\Gamma'$ model was demonstrated to describe these legitimately.[41] The Hamiltonian adopts the following form:

$$\begin{aligned}\mathcal{H} = &\sum_{\langle ij\rangle\parallel\gamma}\left[J\boldsymbol{S}_i\cdot\boldsymbol{S}_j + KS_i^\gamma S_j^\gamma + \Gamma(S_i^\alpha S_j^\beta + S_i^\beta S_j^\alpha)\right]\\ &+\Gamma'\sum_{\langle ij\rangle\parallel\gamma}\left[(S_i^\alpha + S_i^\beta)S_j^\gamma + S_i^\gamma(S_j^\alpha + S_j^\beta)\right]\\ &-\sum_i \boldsymbol{h}\cdot\boldsymbol{S}_i, \end{aligned} \tag{1}$$

where S_i^γ ($\gamma = x, y, z$) is the γ-component of the spin operator at site i. For z bonds, $(\alpha, \beta, \gamma) = (x, y, z)$ with cyclic permutations for x and y bonds. J and K are the isotropic Heisenberg interaction and diagonal Kitaev interaction, respectively. Here, Γ and Γ' are the symmetry-allowed off-diagonal exchanges. The final term in Eq. (1) represents the external magnetic field used to tune the magnetic phase transitions. Conceptually, this is called the [111] magnetic field if $\boldsymbol{h}$ is normal to the honeycomb plane.

The interest in Kitaev materials can be traced back to the synthesis of the $5d^5$ iridates Na_2IrO_3 and α-Li_2IrO_3 shortly after the proposal of the Jackelli–Khaliullin mechanism.[18] By a topotactic replacement of the interlayer alkali Li with hydrogen or silver ions, alternative compositions of $H_3LiIr_2O_6$ and $Ag_3LiIr_2O_6$ have been obtained.[42,43] In parallel, the α-$RuCl_3$ with $4d^5$ configuration is acknowledged as another remarkable Kitaev material. This is because it has an unusually broad low-energy magnetic excitation[44] and hosts a field-induced intermediate-disordered phase.[45–53] Furthermore, research efforts have also identified $3d^7$ materials such as cobaltates $Na_2Co_2TeO_6$, $Na_3Co_2SbO_6$, and $BaCo_2(AsO_4)_2$ as Kitaev materials, although these may have weaker spin–orbit coupling.[21–24] The weak spin–orbit interaction is conducive to the formation of spin–orbit-entangled $J_{\text{eff}} = 1/2$ pseudospins. These are critical for producing Kitaev interactions. Kitaev materials with higher spins have also been proposed. These include spin-1 $X_3Ni_2SbO_6$(X = Li, Na),[27] $Na_3Ni_2BiO_6$,[28] $KNiAsO_6$,[29] and spin-3/2 CrI_3, and $CrXTe_3$(X = Si, Ge).[30–32]

The value of the Kitaev interaction, in conjunction with other terms, differs for different materials. Studies in this field have been developed in conjunction with several appropriate aspects. Prominent examples are the Kitaev-Γ and Γ-Γ' models. We illustrate these models in subsequent sections. In the following, we briefly focus on the pure Kitaev and Γ limits.

2.1. Kitaev Honeycomb Model. The Kitaev honeycomb model consists of bond-directional Ising couplings between nearest-neighbor sites with a quantization axis that depends on the bond type.[13] The Hamiltonian is as follows:

$$\mathcal{H} = \sum_{\langle ij\rangle\parallel\gamma} K_\gamma S_i^\gamma S_j^\gamma, \tag{2}$$

where K_γ is the corresponding coupling constant for each bond type. By rewriting the spin operators using four Majorana fermions $\{b_i^x, b_i^y, b_i^z, c_i\}$ such that $S_i^\gamma = \imath b_i^\gamma c_i/2$, the Hamiltonian in Eq. (2) can be rewritten as follows: $\mathcal{H} = \frac{1}{4}\sum_{\langle ij\rangle\parallel\gamma} b_i^\gamma b_j^\gamma c_i c_j$, Because b_i^γ fermions are local entities, the bond variable $u_{ij} = \imath b_i^\gamma b_j^\gamma$ is a constant of motion that adopts ±1, which is a $\mathbb{Z}_2$-conserved quantity. Therefore, the Hamiltonian can be expressed in a quadratic form: $\mathcal{H} = -\frac{\imath}{4}\sum_{\langle ij\rangle}\langle u_{ij}\rangle c_i c_j$. Evidently, for any given configuration of $\{u_{ij}\}$, the model can be diagonalized exactly. According to Lieb's theorem, the ground state is in a flux-free sector with the hexagonal plaquette operator[13]

$$W_p = 2^6 S_1^x S_2^y S_3^z S_4^x S_5^y S_6^z \tag{3}$$

being +1 for every six-site hexagonal plaquette. Because W_p does not commute with the local spin operators, the ground state cannot display any long-range magnetic order. This indicates that the ground state of the Kitaev model is a type of QSL with exceptionally short-range spin–spin correlations. From the relative intensities of K_γ, fermionic excitations can be gapless (when $|K_x| \le |K_y| + |K_z|$, $|K_y| \le |K_z| + |K_x|$, and $|K_z| \le |K_x| + |K_y|$) or gapped (otherwise).[13]

The isotropic Kitaev model has received considerable attention from both ground state and thermodynamic perspectives. Notwithstanding gapless fermionic excitations owing to itinerant Majorana fermions, the $\mathbb{Z}_2$ vision flux excitations are gapped. The most recent exact calculation yielded a gap energy of $\Delta_v = 0.263313(6)$ K.[54] Moreover, there were two pronounced peaks in the specific heat at well-separated temperature scales. This can be explained by two species of Majorana fermions.[55] The high-temperature crossover driven by itinerant Majorana fermions is intimately connected to the evolution of nearest-neighbor spin correlations. In contrast, low-temperature crossover originates from the thermal fluctuations of fluxes comprising localized Majorana fermions.[55]

2.2. Honeycomb Γ Model. The honeycomb Γ model is a close neighbor of the well-known Kitaev honeycomb model shown in Eq. (2). Owing to the complexity of the interactions in the honeycomb Γ model, it is instrumental for determining the underlying spin patterns of the

ground state at the classical level. By parameterizing each spin as $\hat{\boldsymbol{S}}_n = (\eta_i a, \eta_j b, \eta_k c)$, where $\sqrt{a^2+b^2+c^2} = S$ and $\eta_{i,j,k}$ are independent Ising variables, Rousochatzakis and Perkins determined that the ground-state degeneracy of an N-site cluster is $2^{N/2}$ in addition to the free options of (a, b, c). Therefore, macroscopic degeneracy contributes to the formulation of a classical spin liquid in its ground state.[56] However, the large ground-state degeneracy of the antiferromagnetic (AFM) Γ model is the source of unconventional phases. It can be selected because of the interplay between exchange frustration and competing interactions. Specifically, the four-site zigzag phase displaying a peak at the $\boldsymbol{M}$ point and an 18-site triple-meron crystal[57,58] displaying a peak at the $2\boldsymbol{M}/3$ point belong to the degenerate manifold. The methods used to identify the several common phases in the degenerate manifold are listed in Table 1. We emphasize that when the Γ limit is perturbed using a ferromagnetic (FM) Kitaev interaction, the resultant magnetic ordering is determined to be a triple-meron crystal using the classical Monte Carlo method[57,58] and a machine-learning approach.[59] We also observe that the anisotropy of the Γ term among its three bonds does not disrupt the classical spin-liquid as demonstrated by the Luttinger–Tisza analysis (not shown).

Table 1. Selected degenerate magnetic orderings out of the degenerate manifold of the classical honeycomb Γ model. The number of sites in the unit cell (U.C.), the ordering wave vector $\boldsymbol{Q}$, and the perturbation to pick up this phase are shown correspondingly.

Phase	U.C.	$\boldsymbol{Q}$	Perturb.
AFM phase	2	$\boldsymbol{\Gamma}'$	J, $\Gamma' > 0$
Zigzag phase	4	$\boldsymbol{M}$	$J < 0$
120° phase	6	$\boldsymbol{K}$	$\Gamma' < 0$
Counter-rotating spiral	6	$\boldsymbol{K}$ & $\boldsymbol{\Gamma}'$	$K > 0$
Triple-meron crystal	18	$2\boldsymbol{M}/3$	$K < 0$

The Ising η variables can be split into three interpenetrating triangular sublattices. In the presence of thermal fluctuations, the emergent spherical symmetry at sufficiently high temperatures is lost. This compels spins to primarily point toward one of the six cubic directions. After a suitable finite-size scaling of the plaquette order parameter $\tilde{W}(\boldsymbol{Q}) \propto \sum_p W_p e^{i\boldsymbol{Q}\cdot\boldsymbol{r}_p}$, a hidden plaquette order was revealed in the classical spin-liquid ground state. The temperature-driven thermal phase transitions likely belong to the 2D three-state Potts universality class.[60]

However, the quantum ground state of the honeycomb Γ model is involved. This is because the different methods yield paradoxical results. An exact diagonalization calculation for the 24-site cluster and infinite density-matrix renormalization group (DMRG) study of a cylinder with a width of three unit cells indicated that the ground state is a non-magnetic phase.[61,62] Nevertheless, an infinite DMRG study observed lattice-rotational symmetry breaking. This yielded a nematic paramagnet.[63] In contrast, a variational Monte Carlo simulation indicated that it is a zigzag phase,[64] whereas the pseudofermion functional renormalization group proposed that it is an incommensurate phase displaying peaks near the $2\boldsymbol{M}/3$ point in reciprocal space.[65] Significantly, the incommensurate phase is likely to be a triple-meron crystal because these share a similar landscape in the momentum space. Considering the tendencies of each quantum many-body approach, this may partially explain why different methods target different states. Resolving the quantum ground state puzzle of the honeycomb Γ model, large-scale DMRG calculations were performed on a wide cylinder at 200 sites. The ground state was determined to be gapless ΓSL.[34] The details are reviewed in subsequent sections.

3. Gapless ΓSL is Revealed in the Bond-Modulated Heisenberg-Γ Model. To examine the tendency of zigzag ordering, Luo *et al.* proposed a bond-modulated Heisenberg-Γ model[34] whose Hamiltonian is expressed as

$$\mathcal{H} = \tilde{J} \sum_{\langle ij\rangle\|\gamma} \eta_\gamma \boldsymbol{S}_i \cdot \boldsymbol{S}_j + \Gamma \sum_{\langle ij\rangle\|\gamma} (S_i^\alpha S_j^\beta + S_i^\beta S_j^\alpha), \tag{4}$$

where S_i^γ ($\gamma = x, y, z$) is the γ component of the spin operator. α and β are the remaining two bonds. In conventional XC clusters, $\eta_\gamma = 1$ for horizontal bonds, and -1 for zigzag bonds. The exchange couplings $\tilde{J}$ and Γ are parameterized as follows: $\tilde{J} = \cos\vartheta$ and $\Gamma = \sin\vartheta$ (≥ 0) with $\vartheta \in [0, \pi]$. As ϑ varies, the classical ground state shifts from zigzag to stripy. Here, it passes through a mixed-phase and narrow noncollinear region. DMRG calculations on four XC cylinders with circumferences n ranging from 4 to 10 revealed that the ground-state energy was moderately flat in the middle region and displayed an abrupt down-warping when away from the middle. This indicates that there should be an intermediate region between the zigzag and stripy phases. Significantly, the ground-state energy per site E_g of the honeycomb Γ model was challenging to estimate in that it exhibits nonmonotonic scaling behavior as the circumference n increases. This is similar to that of the Kitaev honeycomb model. However, the energy decreases linearly with the length L_x of the cylinder at each fixed circumference n. From a comparison of the extrapolated energies at achievable circumferences, it can be inferred that the ground-state energy of the honeycomb Γ model is $-0.354(3)$ within the thermodynamic limit.

The magnetic spin structure factor (SSF) $\mathbb{S}_N(\boldsymbol{Q})$ and the associated magnetic order parameter $M_N(\boldsymbol{Q}) = \sqrt{\mathbb{S}_N(\boldsymbol{Q})/N}$, can be used to determine the intervening phase intervals. The zigzag phase peaks at the $\boldsymbol{M}$ point, whereas the stripy phase peaks at both $\boldsymbol{M}$ and $\boldsymbol{M}'$ points [see Fig. 1(a)]. In contrast, the intervening phase displays only a diffuse pattern with soft peaks in its magnetic SSF. This signifies QSL behavior. After an inspection of the DMRG results for both cylinders and hexagonal clusters, it was inferred that the intervening QSL phase persists within the range $\vartheta_{t,l} \leq \vartheta \leq \vartheta_{t,r}$ Here, $\vartheta_{t,l} \simeq 0.50\pi$ and $\vartheta_{t,r} = 0.66(1)\pi$ [see Fig. 1(b)]. At the Γ limit, where $\vartheta = \pi/2$, the magnetization decreases algebraically with circumference n. A linear extrapolation of the maximal peaks yielded a vanishing magnetization. This indicated the QSL phase therein.

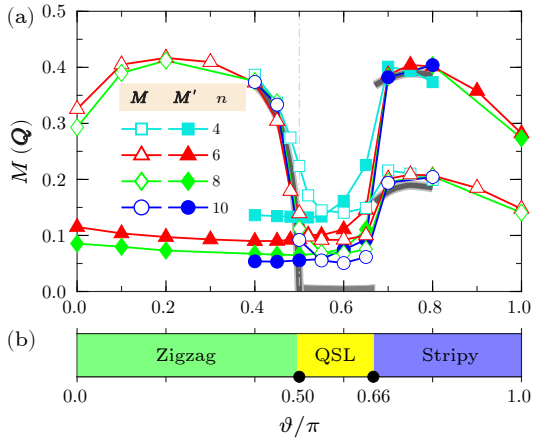

Fig. 1. (a) Magnetic order parameters $M(\boldsymbol{Q})$ for the zigzag order (open symbols) and stripy order (filled symbols) with $\boldsymbol{Q} = \boldsymbol{M}$ and/or $\boldsymbol{M}'$ under four finite XC clusters. The thick gray line shows the magnetic order in the thermodynamic limit. (b) Quantum phase diagram of the bond-modulated $\tilde{J}$-Γ model, which contains the zigzag phase, QSL, and stripy phase.[34]

The excitation gaps $\Delta_v = E_v - E_g$ exhibited distinguishing behaviors in the magnetically ordered and QSL phases. In a 24-site hexagonal cluster, both zigzag and stripy phases have doubly degenerate ground states. Thus, Δ_1 is vanishing small, whereas Δ_2 increases. However, the ground state of the intermediate QSL phase is unique, and the density of state in the low-energy spectrum is higher than that with its neighbor gapped phases. This collapse of the excitation gaps can be interpreted as a signature of gapless spectrum. The fact that the lowest excitation gap at $\vartheta = \pi/2$ decreased from 0.08656249 ($N = 24$) to 0.04009844 ($N = 32$) is also consistent with a critical system.

The von Neumann entanglement entropy $\mathcal{S}_{\rm vN}$ is another versatile tool for diagnosing the quantum criticality. The entanglement entropy exhibits a striking difference depending on the cylinder width. On a three-leg cylinder, $\mathcal{S}_{\rm vN}$ is exceedingly insensitive to the length. This reveals a zero central charge. In contrast, $\mathcal{S}_{\rm vN}$ increases with the length of the four-leg cylinder, and the logarithmic fitting of $\mathcal{S}_{\rm vN}$ with respect to the length L_x yields a central charge of approximately three. With regard to the characteristic of QSL, the fact that the central charge is highly dependent on the width of the cylinders may 1) imply the presence of a spinon Fermi surface whose pockets can be detected by different cuts in the Brillouin zone or 2) indicate a Dirac QSL with three Dirac Fermions around $\boldsymbol{M}$ points. Considered in combination, the vanishing magnetization, collapsing excitation gaps, and width-dependent central charge on the long cylinders indicate that the ground state of the honeycomb Γ model is a feasible gapless QSL.

4. Spin-1 Kitaev-Γ Model. The Kitaev-Γ model has captured significant attention because of its relevance to real materials and its capability to harbor exotic phases. Applying the perturbation theory to a five-orbital Hubbard model and utilizing the energy bands via *ab initio* calculations,[66] it is proposed that the effective Hamiltonian of α-$RuCl_3$ is the Kitaev-Γ model whose Hamiltonian is

$$\mathcal{H} = \sum_{\langle ij\rangle\|\gamma} \left[K S_i^\gamma S_j^\gamma + \Gamma (S_i^\alpha S_j^\beta + S_i^\beta S_j^\alpha) \right]. \tag{5}$$

After fitting the inelastic neutron-scattering data to the dynamic SSF, the exchange couplings were estimated to be $K = -6.8\,\text{meV}$ and $\Gamma = 9.5\,\text{meV}$.[51,66] Although a convincing model describing α-$RuCl_3$ remains unclear,[33] this model is widely considered to be a reasonable starting point for understanding the field-induced intermediate phase and nontrivial thermal Hall conductivity. Theoretically, notwithstanding its simplicity, the full phase diagram of the Kitaev-Γ model with the FM Kitaev interaction is not understood completely because of the strong frustration.[61–65] Starting from the FM Kitaev limit, the phase that appears next to the Kitaev QSL remains unclear. A few studies have identified a ferromagnet based on the peak at the center of the first Brillouin zone. For a review, see Ref. [17]. Motivated by the synthesis of high-spin Kitaev magnets, it is necessary to study quantum phase transitions (QPTs) for $S > 1/2$, i.e., $S = 1$.

4.1. Chiral Spin State in Nonfrustrated Regions. Classically, the ground state of a nonfrustrated region can be understood conveniently by systematically analyzing the spin patterns. First, it is advantageous to select and parameterize the central spin as $\boldsymbol{S}_0 = (\eta_a a, \eta_b b, \eta_c c)$. Here, $(\eta_a,\ a)$ [$(\eta_b,\ b)$ and $(\eta_c,\ c)$, respectively] denote the sign and intensity of S_0^x (S_0^y and S_0^z, respectively). Here, $\sqrt{a^2+b^2+c^2} = S$ and ηs are independent Ising variables that can be ± 1. Considering the peculiar structures of the Kitaev and Γ interactions, the three neighbor spins can be formulated as $\boldsymbol{S}_i = -(\eta_a a, \eta_c c, \eta_b b)$ (for $\boldsymbol{X}$ bond), $\boldsymbol{S}_j = -(\eta_c c, \eta_b b, \eta_a a)$ (for $\boldsymbol{Y}$ bond). and $\boldsymbol{S}_k = -(\eta_b b, \eta_a a, \eta_c c)$ (for $\boldsymbol{Z}$ bonds). Thus, the entire spin texture can be generated accordingly. This results in a $(2+6)$-ordering (the digits here represent the number of sites in the unit cells) that encompasses a two-sublattice AFM phase and six-sublattice counter-rotating spiral order. One should note that the AFM phase occurs only when $\eta_a = \eta_b = \eta_c = \pm 1$ and $a = b = c = S/\sqrt{3}$. Meanwhile, the spins in the counter-rotating spiral order rotate clockwise in one of the two sublattices, whereas the remaining spins on the other sublattice rotate counterclockwise around the [111] axis.[67] Because there are only three η values, the ground-state degeneracy is eight for any fixed selection of $\{a, b, c\}$. Notwithstanding the many possibilities for $\{\eta_a, \eta_b, \eta_c\}$ and $\{a, b, c\}$, the classical ground-state energy per site is $e_{\rm cl} = -(\Gamma + K/2)S^2$.

The counter-rotating spiral order can also be understood using the hidden SU(2) point. To reveal this, it is essential to adopt a six-sublattice $\mathcal{T}_6$ transformation. It comprises the cyclic (anti-cyclic) permutations among the spin components at odd (even) sites within a unit cell.[68] Considering the $\mathcal{T}_6$ transformation, the Hamiltonian in Eq. (5) is rotated as follows:

$$\tilde{\mathcal{H}} = -\Gamma \sum_{\langle ij\rangle} \tilde{S}_i \cdot \tilde{S}_j + (\Gamma - K) \sum_{\langle ij\rangle\|\gamma} \tilde{S}_i^\gamma \tilde{S}_j^\gamma, \tag{6}$$

where the first term is the FM Heisenberg interaction and the second is the refined Kitaev interaction. Note that

the types of Ising bonds are redistributed after rotation, thereby reformulating the Kekulé-type pattern. Specifically, $\tilde{\boldsymbol{X}}$ bonds were oriented outside, whereas $\tilde{\boldsymbol{Y}}$ and $\tilde{\boldsymbol{Z}}$ bonds alternated along a benzene-like ring. When K and Γ are equal, Eq. (6) is reduced to the SU(2)-symmetric FM Heisenberg model. The counter-rotating spiral order transitioned to a dual FM phase after rotation.

It is predicable that quantum fluctuations may constrain the selection of $\{a, b, c\}$. Second-order calculations using the real-space perturbation theory revealed that the leading energy correlation is[17]

$$e_{\rm cl}^{(2)} = -\frac{(\Gamma-K)^2 S}{32|\Gamma+2K|}\left[\left(\frac{a}{S}\right)^4+\left(\frac{b}{S}\right)^4+\left(\frac{c}{S}\right)^4\right]. \quad (7)$$

Thus, when $K \neq \Gamma$, the total energy is minimized when one of the elements in $\{a, b, c\}$ is S and the others are zero. In addition, only one of the ηs that adheres to the nonzero element survives. This result can be verified independently using the linear spin-wave theory, where the spin wave energy has a minimal value at six points on the cubic axes.

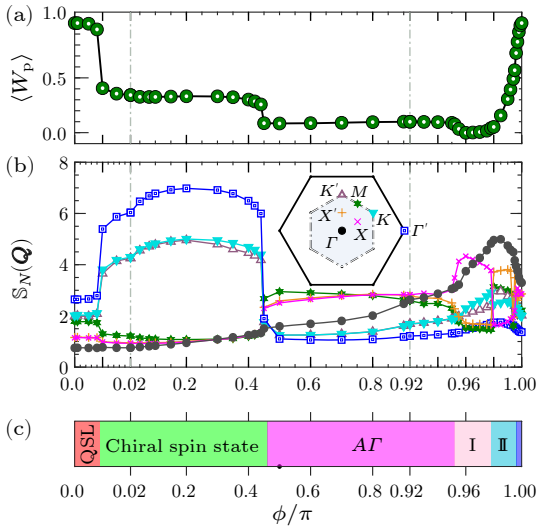

Fig. 2. (a) The flux-like density $\langle \overline{W}_p \rangle$ as a function of ϕ on the 24-site hexagonal cluster. (b) The static SSF $\mathbb{S}_N(\boldsymbol{q})$ at high-symmetry points shown in the reciprocal space (see inset). (c) The quantum phase diagram of the spin-1 Kitaev-Γ model. The acronym $A\Gamma$ denotes an antiferromagnetic Γ phase. The symbols I and II represent two nematic ferromagnets.[35] Copyright 2024, American Physical Society.

At the quantum level, the emergent continuous symmetry is broken down into a discrete symmetry and has a noteworthy constraint on the magnetic order and scalar spin chirality. It can be verified conveniently that $M(\boldsymbol{\Gamma}') = S/2$ and $M(\boldsymbol{K}) = S/\sqrt{6}$. This implies that $M(\boldsymbol{K})/M(\boldsymbol{\Gamma}') = \sqrt{6}/3 \approx 0.8165$. As shown in Fig. 2(b), this relationship was verified by DMRG calculations.[35] The scalar spin chirality is defined as

$$\hat{\chi}_{ijk}^{\triangle} = \hat{\boldsymbol{S}}_i \cdot (\hat{\boldsymbol{S}}_j \times \hat{\boldsymbol{S}}_k), \quad (8)$$

where sites (i, j, k) are three neighboring sites belonging to the same sublattice. It follows that $|\chi_{ijk}| = S^3$ (the saturation value) because the three spins are perpendicular to each other. From this perspective, the underlying phase is termed a magnetically ordered chiral spin state. In addition, the chiral spin state has a specific columnar-like or plaquette-like dimer covering depending on the relative values of K and Γ. The hexagonal plaquette operator experiences the trimerization phenomenon. Moreover, the flux-like density $\langle \bar{W}_p \rangle = \langle \hat{W}_p \rangle / N_p$ ($N_p = N/2$) was determined to be $-1/3$ and $1/3$ for the spin-1/2 and spin-1 cases, respectively [see Fig. 2(a)].

4.2. Nematic Ferromagnets in the Frustrated Regions. Determining the ground state phase diagram near the FM Kitaev limit is exceptionally challenging. Using the von Neumann entropy and flux-like density, it is observed that two distinct intervals are neighbors near the Kitaev QSL. The SSFs have a dominant peak at the $\boldsymbol{\Gamma}$ point and subleading peaks at the $\boldsymbol{K}/2$ and $\boldsymbol{K}'/2$ points. Because there are two $\boldsymbol{K}$ and $\boldsymbol{K}'$ points in the Brillouin zone, it should be noted that the specific positions of the subleading peaks are different in the two phases. This discrepancy can be used to distinguish one from another and to designate the likelihood of C_3 rotational symmetry breaking. Coincidentally, the energies of the three bonds in each phase differed significantly. This revealed a finite lattice nematicity defined as $\mathcal{O}_{\rm NF} = |\min(E^\gamma) - \max(E^\gamma)|$.

The magnetic order parameter $M_N(\boldsymbol{\Gamma})$ and nematic order parameter $\mathcal{O}_{\rm NF}$ are amenable to identifying the characteristics of the phases. By calculating $M_N(\boldsymbol{\Gamma})$ for four rhombic clusters with the total number of sites ranging from 12 to 32, the magnetic order parameter for each exchange parameter was estimated as a finite value within the thermodynamic limit. However, although the extrapolation of $\mathcal{O}_{\rm NF}$ is not feasible, we observed that $\mathcal{O}_{\rm NF}$ was robust against the geometry and site number of the cluster. This evidence indicates that these phases are nematic ferromagnets. However, the major difference between the two is still unclear and needs to be studied more extensively.

Finally, we wish to note that it is also worthwhile to study the parameter space in which $\Gamma < 0$. Classically, by rotating $\boldsymbol{S}_i \to -\boldsymbol{S}_i$ in a single sublattice, we send $\theta \to \pi+\theta$ Thus, one can focus only on $\Gamma > 0$. However, this transformation is not applicable to quantum cases. Therefore, it is worthwhile to evaluate potential novel phases at the quantum level for a negative Γ term.

5. Γ-Γ' Model: With and Without Magnetic Field. Because both Γ and Γ' interactions are off-diagonal exchange couplings, the Γ-Γ' model is likely to host exotic states of matter owing to the interplay between exchange frustration and competing interactions. Although this model is anisotropic, it can be rewritten as an easy-axis XXZ model with $\mathbb{Z}_2 \ltimes U(1)$ symmetry when $\Gamma = \Gamma'$. This indicates that the AFM and FM phases can exist conditionally in the ground state. At the classical level, the entire phase diagram can be mapped using the Lutinger–Tisza method. There are four different phases, in which two of them are out-of-plane AFM phase (when $\Gamma' > 0$) and FM phase (when $\Gamma' < 0$) while the other two are distinct in-plane 120° phases.[37] Because the energy of the AFM phase is

$-(\Gamma+2\Gamma')$ and that of the 120° phases is $-|\Gamma-\Gamma'|$, it is inferred that a first-order phase transition occurs between the 120°-phase and AFM phase by switching the sign of the Γ' interaction in the dominant Γ-region. However, even within the framework of the linear spin-wave theory, strong quantum fluctuations would alter the underlying phases and QPTs dramatically. It is observed that the spin-wave energy of the zigzag phase is lower than that of the 120° phase. This implies that the zigzag phase may replace the 120° phase in the region of $\Gamma' < 0$. However, the energy reduction of the AFM phase is insufficient compared with that of the zigzag phase in the vicinity of the Γ limit. Nonetheless, magnon instability of the second phase occurs when Γ' becomes positive. This indicates the presence of an intermediate region between the two magnetically ordered states.[36]

5.1. Chiral-Spin Ordering. Two exotic phases are observed in the intermediate region. Here, ΓSL protrudes from the pure Γ-limit. Meanwhile, the other is chiral spin ordering with a spontaneously broken time-reversal symmetry (TRS).[36] Chiral-spin ordering is characterized by the nonzero scalar spin chirality defined in Eq. (8). Depending on the presence of a lattice site in the center of the triangle, the chirality can be classified into two types: χ_p (if centered at a site) and χ_n (if inside a hexagon). For both the types, the scalar spin chirality is distributed uniformly in the two sublattices but with different signs. In addition, χ_p and χ_n have the same sign but different values within each sublattice.

Because of TRS breaking, the ground state of the chiral spin ordering is doubly degenerate, and its static SSF exhibits a soft peak at the corner of the second Brillouin zone. In addition to the degenerate ground states, the lowest excitation gap varies from 0.11207 (24-site) to 0.00012 (32-site) for the hexagonal clusters for a gapless excitation within the thermodynamic limit. By calculating the entanglement entropy of the three-legged cylinder, the central charge was estimated to be approximately one. Thus, the vanishing excitation gap and finite central charge together support the presence of gapless excitations in chiral spin ordering. In addition, as the system size increased, the magnetic order parameter vanished after an appropriate extrapolation of the system size. This indicated that the chiral spin ordering was magnetically disordered.

A noteworthy question is whether the chiral spin ordering is a QSL. The dynamic SSF calculation reveals a broad continuous feature in the low-frequency region. This is likely to be an evidence of the QSL phase. However, the modular $\mathcal{S}$ matrix constructed from minimal entangled states is trivial in violation of the topological order. However, it is in line with TRS-breaking chiral-spin ordering with short-range entanglement. Hence, further studies are required to elucidate the characteristic of chiral spin ordering.

5.2. Spin-Flop Phase. By switching on the [111] magnetic field, a spin-flop phase was identified as being sandwiched between the low-field phases and the paramagnetic phase in a large field (cf. Fig. 3.) Starting from the AFM phase, the spin-wave analysis predicts that the spin-flop phase is situated in the field interval $\sqrt{3}(\Gamma+2\Gamma') < h/S < 3(\Gamma+2\Gamma')$.[37] A spin flop refers to a first-order transition in which the ground state transitions from an AFM ordering to an umbrella-like state where the spins exhibit components that are normal to the field direction. It is noteworthy that the in-plane components are distributed uniformly, thus displaying temporary emergent $U(1)$ symmetry. Nevertheless, the in-plane magnetization was unstable against additional perturbations, and the continuous symmetry broke down into a discrete C_3 rotational symmetry accompanied by gapless Goldstone modes. DMRG calculations indicated that the excitation gaps were small and that the spectrum was rather dense. This, in turn, implied gapless excitation in the spin-flop phase. When $\Gamma' = \Gamma$, the Γ-Γ' model in the [111] magnetic field is equivalent to an easy-axis XXZ antiferromagnet subjected to a longitudinal magnetic field. By an appropriate mapping, it can be re-expressed as an extended Bose–Hubbard model within the hard core limit. Therefore, the spin-flop phase is also acknowledged as a superfluid phase in bosonic languages.

Before concluding, we note that by exerting an in-plane magnetic field on the Γ-Γ' model, two spin-flop phases appeared over the AFM and FM phases. Depending on the relative value of the two exchange couplings as well as the strength and direction of the magnetic field, it is demonstrated that within each spin-flop phase, there are at least three topologically distinct regions. Here, the Chern number of the lowest magnon band belongs to the set $\{+1, 0, -1\}$.[69]

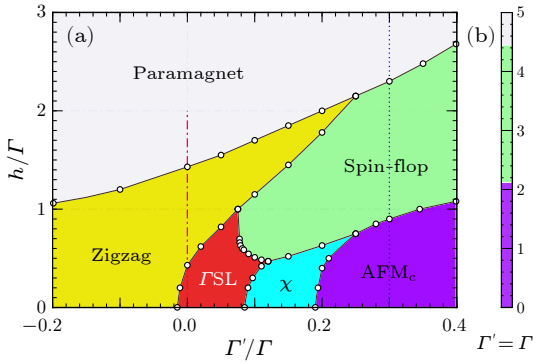

Fig. 3. Quantum phase diagram of the Γ-Γ' model in a [111] magnetic field. In the zero field, it contains the zigzag phase, ΓSL, chiral-spin ordering (marked by the symbol χ), and AFM phase. An intermediate spin-flop phase and a paramagnetic phase originate when the magnetic field is increased.[37] Copyright 2022, American Physical Society.

6. Anisotropic Kitaev-Γ Chain. Confronted with difficulties in obtaining convincing phase diagrams of the honeycomb-lattice Kitaev-Γ model, research efforts have also been applied to 1D physics to capture referable indications. The full Hamiltonian of the bond-alternating Kitaev-Γ chain is

$$\mathcal{H} = \sum_{l=1}^{L/2} g_x \mathcal{H}^{(x)}_{2l-1,2l}(\theta) + g_y \mathcal{H}^{(y)}_{2l,2l+1}(\theta), \tag{9}$$

where the exchange term for each bond is given by

$$\mathcal{H}_{i,j}^{(\gamma)}(\theta) = KS_i^\gamma S_j^\gamma + \Gamma(S_i^\alpha S_j^\beta + S_i^\beta S_j^\alpha). \quad (10)$$

Here, L is the length of the chain, and g_x (g_y) denotes the strength of the odd(even) bond. By appropriate spin rotations, it can be verified conveniently that the model has two unique properties that strongly constrain the phase diagram landscape. The first is the self-duality relationship. It implies that each eigenvalue E of $\mathcal{H}$ satisfies $E(g) = gE(1/g)$. Here, $g \equiv g_y/g_x$ is the relative bond strength. The other is a mirror relationship that yields $E(K, \Gamma) = E(K, -\Gamma)$.[38]

Furthermore, a six-sublattice rotation is amenable to revealing hidden SU(2) symmetry in the model when K and Γ are of equal strength. Under this transformation, the Hamiltonian is expressed in the following diagonal form:

$$\tilde{\mathcal{H}}_{i,j}^{(\gamma)}(\theta) = -K\tilde{S}_i^\gamma \tilde{S}_j^\gamma - \Gamma(\tilde{S}_i^\alpha \tilde{S}_j^\alpha + \tilde{S}_i^\beta \tilde{S}_j^\beta), \quad (11)$$

where $\gamma = \tilde{x}$, $\tilde{z}$, and $\tilde{y}$ are circular.[70] After parameterizing $\Gamma = \cos\theta$ and $K = \sin\theta$, quantum phase diagrams of the spin-1/2 and the spin-1 Kitaev-Γ chains are shown in Figs. 4(a) and 4(b), respectively.

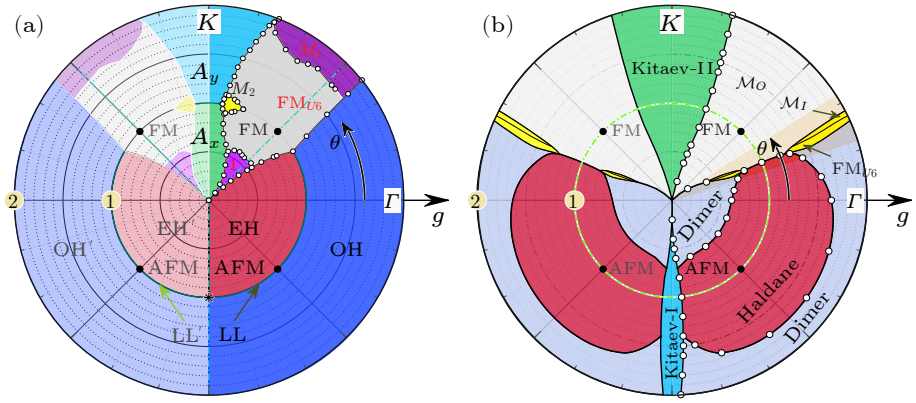

Fig. 4. (a) Quantum phase diagram of the spin-1/2 Kitaev-Γ chain. There are three magnetically ordered states, namely, the FM_{U_6} phase, M_1 phase, and M_2 phase. Furthermore, there are four magnetically disordered states, namely, the A_x and A_y phases and the even-Haldane (EH) and odd-Haldane (OH) phases. (a) Quantum phase diagram of the spin-1 Kitaev-Γ chain. It contains the FM_{U_6} phase, the $\mathcal{M}_I$ phase, $\mathcal{M}_O$ phase, the dimerized phase, the Haldane phase, and two distinct Kitaev phases.[38,39] Copyright 2021, American Physical Society.

6.1. The $S = 1/2$ Case. The spin-1/2-bond-alternating Kitaev-Γ chain has a rich phase diagram and hosts seven distinct phases. These phases can be classified into three categories based on their preferential interactions.[38] First, in the absence of the Γ term, the model is reduced to the Kitaev spin chain. It is known to undergo topological QPT between the gapped A_x and A_y phases at $g = 1$. On the AFM Kitaev side, the regions of the A_x and A_y phases are enlarged by exerting Γ interactions. In contrast, these phases disappear immediately when the sign of the Kitaev interaction is negative. Second, when $\theta = -\pi/4$ ($K = -|\Gamma|$), the model is a bond-alternating spin-1/2 Heisenberg chain that hosts two gapped disordered states with different nonlocal string order parameters as long as $g \neq 1$. The ground state is an odd (even) Haldane phase when $g > 1$ ($g < 1$). The transition between the two is continuous with a central charge $c = 1$. From a topological perspective, the odd-Haldane phase has fractional spin-1/2 edge states and is acknowledged as a symmetry-protected topological phase.

There are three magnetically ordered states in the vicinity of the hidden FM Heisenberg point where $K = |\Gamma|$. Near the isotropic limit, there is an FM_{U_6} phase with $O_h \to D_4$ symmetry breaking. It results in six-fold degenerate ground states with moments along the $\pm\hat{x}$, $\pm\hat{y}$, and $\pm\hat{z}$ spin directions.[70] For example, a moment within a unit cell can be expressed as

$$(\langle\tilde{\boldsymbol{S}}_1\rangle, \langle\tilde{\boldsymbol{S}}_2\rangle, \langle\tilde{\boldsymbol{S}}_3\rangle; \langle\tilde{\boldsymbol{S}}_4\rangle, \langle\tilde{\boldsymbol{S}}_5\rangle, \langle\tilde{\boldsymbol{S}}_6\rangle) = (c, b, b; c, a, a)\hat{z}, \quad (12)$$

where a, b, and c are the magnitudes of the spin ordering along the $\hat{z}$ direction and a, b, $c \leq S$. When approaching the Kitaev side, an M_2-phase exists with a spin-nematic correlation.[38,71] During large bond alternations, a magnetically ordered phase with eight-fold ground-state degeneracy exists. These degenerate states can be unified using the η notation.[56] From this, the spins within the six-site unit cell are

$$\begin{pmatrix}\langle\tilde{\boldsymbol{S}}_1\rangle\\ \langle\tilde{\boldsymbol{S}}_2\rangle\\ \langle\tilde{\boldsymbol{S}}_3\rangle\end{pmatrix}^T = \left[\begin{pmatrix}\eta_x a\\ \eta_y b\\ \eta_z c\end{pmatrix}, \begin{pmatrix}\eta_x a\\ \eta_y c\\ \eta_z b\end{pmatrix}, \begin{pmatrix}\eta_x c\\ \eta_y a\\ \eta_z b\end{pmatrix}\right], \quad (13)$$

and

$$\begin{pmatrix}\langle\tilde{\boldsymbol{S}}_4\rangle\\ \langle\tilde{\boldsymbol{S}}_5\rangle\\ \langle\tilde{\boldsymbol{S}}_6\rangle\end{pmatrix}^T = \left[\begin{pmatrix}\eta_x b\\ \eta_y a\\ \eta_z c\end{pmatrix}, \begin{pmatrix}\eta_x b\\ \eta_y c\\ \eta_z a\end{pmatrix}, \begin{pmatrix}\eta_x c\\ \eta_y b\\ \eta_z a\end{pmatrix}\right]. \quad (14)$$

Here, a, b, c (≥ 0) satisfy the constraint $\sqrt{a^2+b^2+c^2} \leq S$. Meanwhile, η_x, η_y, η_z ($= \pm 1$) are the Ising variables. The three η's have the flexibility to select 1 or -1 without altering the energy. This generates a degenerate manifold.

6.2. The $S = 1$ Case. Similar to the spin-1/2 case, the spin-1 bond-alternating Kitaev-Γ chain also displays

a phase diagram with seven distinct phases.[39] In the Kitaev limit, there are two gapped Kitaev phases that survive finite but different values of the Γ interaction. Consequently, the region of the Kitaev phase near the FM Kitaev limit is significantly smaller than that on the AFM Kitaev side. The ground states of the Kitaev phases are unique under periodic boundary conditions. Meanwhile, these are four-fold degenerate under open boundary conditions. This is analogous to that of the Haldane phase. However, the fact that the lowest entanglement spectra in the Kitaev phase are unique is inconsistent with the symmetry-protected topological phase. By increasing the Γ-interaction from the FM Kitaev limit, the Haldane phase appears when the bond alternation is modest, and the dimerized phase is induced in the presence of a large anisotropy. Furthermore, three distinct magnetically ordered states (M_O, M_I, and FM_{U_6}) are favored when Γ and Kitaev interactions are comparable and the second is AFM. The M_O phase has eight-fold ground-state degeneracy and exhibits the pattern shown in Eq. (13) and Eq. (14). In addition, the extent of the M_O phase is significantly larger than those of the M_I and FM_{U_6} phases.

Although the spin-1 Kitaev chain is not solvable, it has an analog of $\mathbb{Z}_2$-valued conserved quantities on the bond. The ground state is located in the flux-free sector, where all the $\mathbb{Z}_2$ quantities are unitary. Meanwhile, the degeneracy of the first excited state is equal to the number of sites in the chain. This corresponds to the flipping sign of the arbitrary $\mathbb{Z}_2$ quantities. Owing to these unusual excitations, the Kitaev phase displays a nontrivial double-peak structure at specific heat. Unlike the spin-1/2 Kitaev honeycomb model, whose low-temperature peak originates from the freezing of vison fluxes, the low-temperature peak in the spin-1 Kitaev chain is related to the freezing of $\mathbb{Z}_2$ quantities and is relevant to the highly degenerate low-lying excited states. Moreover, thermal entropy is released gradually without generating a plateau in the crossover temperature region. This differs from the Kitaev honeycomb model.

6.3. Insights of the Kitaev Phase. As shown in Fig. 4(b), the bond alternation cannot induce QPT in the pure Kitaev limit. However, the Kitaev phase is replaced by a spontaneous symmetry-breaking phase when the single-ion anisotropy (SIA) is introduced. To interpolate the [001]- and [111]-type SIAs, the Kitaev phase can be perturbed using the following term:[40]

$$\mathcal{H}_{\mathrm{SIA}} = D\sum_{i=1}^{L}\left[\frac{\sin\vartheta}{\sqrt{2}}(S_i^x + S_i^y) + \cos\vartheta S_i^z\right]^2, \qquad (15)$$

where $D \leq 0$ and $\vartheta \in [0, \pi/2]$. The full Hamiltonian acknowledges a TRS, a dihedral symmetry, a translational symmetry, etc. This enables spontaneous symmetry-breaking phases to occur. In a Kitaev chain with a [001]-type SIA (i.e., $\vartheta = 0$) or [111]-type SIA [i.e., $\vartheta = \tan^{-1}(\sqrt{2})$], the ground state undergoes QPT to the dimerized or AFM phase at $D = -0.6551(2)$ or $D = -0.6035(2)$, respectively. Both QPTs belong to the Ising universality class, in which the central charge $c = 1/2$ and the critical exponents $\beta = 1/8$ and $\nu = 1$. The dimerized phase breaks the translational symmetry, whereas the AFM phase breaks the TRS and dihedral symmetry. Thus, these can only exhibit a first-order QPT in Landau's paradigm. However, for a sufficiently large SIA, the dimerized phase and AFM phase is observed to undergo a "Landau-forbidden" continuous QPT with a central charge $c = 1$. This indicates that the spin-1 Kitaev chain can serve as a platform for supporting deconfined quantum criticality.

Depending on the intensity and angle of the SIA, the Kitaev phase can be classified into two types. However, it is characterized by a unique ground state under periodic boundary conditions. The degeneracy of the first excited state can be unique or double. The first excited ground state is unique over a wide area (e.g., in the region around the path of the [111]-type SIA), compared with the two-fold situation observed in a particular area where $|D|$ and ϑ are small. From this perspective, the Kitaev phases can be classified into type I and type II because of the degeneracy of the first excited state. Because the lowest excitation gap of the Kitaev phase never closes over its entire area, the variation between the two types is regarded as a crossover rather than a QPT. These two types can also be distinguished by the spatial distribution of the bond parity operator $\hat{W}_l$ in their energy spectra. Although $\hat{W}_l$ is completely flat in the ground state, owing to the absence of translational symmetry breaking, it varies smoothly in type-I. However, it undergoes rapid oscillation in type-II in the excited states.

Notwithstanding the differentiation in the Kitaev phase, the hallmark of its ground state is that it involves a spin-nematic order parameter $\mathcal{O}_{\mathrm{SN}}$ It can be extracted from the four-spin correlation function:

$$Q_1(i, j) = \langle S_i^+ S_{i+1}^+ S_j^- S_{j+1}^-\rangle \simeq \mathcal{O}_{\mathrm{SN}}^2 e^{-\imath\phi}, \qquad (16)$$

where ϕ denotes the phase factor that varies as the strength of the interaction does. Because the Kitaev phase preserves the translational symmetry and TRS, $Q_1(r) \equiv Q_1(i, j)$ with $r = |j - i|$. It is observed that $Q_1(r)$ has a strong even-odd effect. Here, ϕ is finite when r is odd and vanishes otherwise. For a specific cut along the line of the [111]-type SIA, the nontrivial ϕ varies from π to zero when $|D|$ exceeds the pure Kitaev limit. It is noteworthy that it underwent a rapid variation near the quantum-critical region. The derivatives of ϕ with respect to D, $\partial\phi/\partial D$, diverges at the quantum critical point as the chain length approaches infinity. This indicates that the phase factor ϕ related to $Q_1(r)$ (r is odd) can function as a tool for examining the QPT.

7. Summary and Perspectives. We have reviewed a few numerical works related to exotic phases and quantum phase diagrams in Kitaev-Γ and Γ-Γ' models. Both of these are specific cases of the generic $JK\Gamma\Gamma'$ model. Unlike the long-standing SU(2)-symmetric models, these models have only discrete symmetries. This makes it exceptionally difficult to handle a sufficient system size and simultaneously achieve an effective numerical precision. Notwithstanding these challenges, many noteworthy

phases can be identified, including QSLs. Although these studies do not necessarily resolve all the conundrums, these demonstrated that the spin-orbit coupled model provides a productive platform for evaluating unconventional phases of matter and comprehending collective emergent quantum phenomena.

Beyond the scope of the current overview, several intriguing and challenging issues remain unaddressed. First, in the spin-1/2 AFM Kitaev model of a honeycomb lattice, the fate of the Kitaev QSL in the presence of a [111] magnetic field is a topic of considerable interest. Moreover, the number and characteristic of the intermediate phases before entering the trivial polarized phase are under debate.[72–77] Second, although the ground state of the spin-1 Kitaev honeycomb model is widely considered to be a QSL, whether the excitations are gapped or gapless is still unclear.[78–81] Third, similar to the spin-1/2 analog, it would also be noteworthy to determine the characteristic of the field-induced intermediate phase in the spin-1 AFM Kitaev model.[82–84] Finally, it is necessary to propose a Hamiltonian that undergoes an in-plane field-induced QSL phase on top of a zigzag ordering in a multidimensional $JK\Gamma\Gamma'$ parameter space.

Acknowledgements. We thank Ken Chen, Jacob S. Gordon, Shijie Hu, Jinbin Li, Xudong Li, Ahmed Rayyan, P. Peter Stavropoulos, Bin Xi, and Zongsheng Zhou for the collaboration on related topics, particularly Hae-Young Kee. This study was supported by the National Program on Key Research Projects (Grant No. MOST2022YFA1402700), the National Natural Science Foundation of China (Grant Nos. 12304176, 12274187, 12247183, and 12247101), and the Natural Science Foundation of Jiangsu Province (Grant No. BK20220876). The computations were partially supported by the High-Performance Computing Platform of Nanjing University of Aeronautics and Astronautics.

References

[1] Balents L 2010 *Nature* **464** 199
[2] Zhou Y, Kanoda K, and Ng T K 2017 *Rev. Mod. Phys.* **89** 025003
[3] Wen J, Yu S L, Li S, Yu W, and Li J X 2019 *npj Quantum Mater.* **4** 12
[4] Broholm C, Cava R J, Kivelson S A, Nocera D G, Norman M R, and Senthil T 2020 *Science* **367** eaay0668
[5] Anderson P W 1973 *Mater. Res. Bull.* **8** 153
[6] Wen X G 2017 *Rev. Mod. Phys.* **89** 041004
[7] Liao H J, Xie Z Y, Chen J, Liu Z Y, Xie H D, Huang R Z, Normand B, and Xiang T 2017 *Phys. Rev. Lett.* **118** 137202
[8] Zhang C and Li T 2020 *Phys. Rev. B* **102** 195106
[9] Hu S, Zhu W, Eggert S, and He Y C 2019 *Phys. Rev. Lett.* **123** 207203
[10] Gong S S, Zheng W, Lee M, Lu Y M, and Sheng D N 2019 *Phys. Rev. Lett.* **100** 241111(R)
[11] Wang L and Sandvik A W 2018 *Phys. Rev. Lett.* **121** 107202
[12] Liu W Y, Gong S S, Li Y B, Poilblanc D, Chen W Q, and Gu Z C 2022 *Sci. Bull.* **67** 1034
[13] Kitaev A 2006 *Ann. Phys.* **321** 2
[14] Hermanns M, Kimchi I, and Knolle J 2018 *Annu. Rev. Condens. Matter Phys.* **9** 17
[15] Takagi H, Takayama T, Jackeli G, Khaliullin G, and Nagler S E 2019 *Nat. Phys. Rev.* **1** 264
[16] Trebst S and Hickey C 2022 *Phys. Rep.* **950** 1
[17] Rousochatzakis I, Perkins N B, Luo Q, and Kee H Y 2024 *Rep. Prog. Phys.* **87** 026502
[18] Jackeli G and Khaliullin G 2009 *Phys. Rev. Lett.* **102** 017205
[19] Singh Y and Gegenwart P 2010 *Phys. Rev. B* **82** 064412
[20] Sears J A, Songvilay M, Plumb K W, Clancy J P, Qiu Y, Zhao Y, Parshall D, and Kim Y J 2015 *Phys. Rev. B* **91** 144420
[21] Songvilay M, Robert J, Petit S, Rodriguez-Rivera J A, Ratcliff W D, Damay F, Balédent V, Jiménez-Ruiz M, Lejay P, Pachoud E, Hadj-Azzem A, Simonet V, and Stock C 2020 *Phys. Rev. B* **102** 224429
[22] Lin G, Jeong J, Kim C *et al.* 2021 *Nat. Commun.* **12** 5559
[23] Li X, Gu Y, Chen Y, Garlea V O, Iida K, Kamazawa K, Li Y, Deng G, Xiao Q, Zheng X, Ye Z, Peng Y, Zaliznyak I A, Tranquada J M, and Li Y 2022 *Phys. Rev. X* **12** 041024
[24] Zhong R, Gao T, Ong N P, and Cava R J 2020 *Sci. Adv.* **6** eaay6953
[25] Ji J, Sun M, Cai Y, Wang Y, Sun Y, Ren W, Zhang Z, Jin F, and Zhang Q 2021 *Chin. Phys. Lett.* **38** 047502
[26] Stavropoulos P P, Pereira D, and Kee H Y 2019 *Phys. Rev. Lett.* **123** 037203
[27] Zvereva E A, Stratan M I, Ovchenkov Y A, Nalbandyan V B, Lin J Y, Vavilova E L, Iakovleva M F, Abdel-Hafiez M, Silhanek A V, Chen X J, Stroppa A, Picozzi S, Jeschke H O, Valentí R, and Vasiliev A N 2015 *Phys. Rev. B* **92** 144401
[28] Shangguan Y, Bao S, Dong Z Y, Xi N, Gao Y P, Ma Z, Wang W, Qi Z, Zhang S, Huang Z *et al.* 2023 *Nat. Phys.* **19** 1883
[29] Taddei K M, Garlea V O, Samarakoon A M, Sanjeewa L D, Xing J, Heitmann T W, dela Cruz C, Sefat A S, and Parker D 2023 *Phys. Rev. Res.* **5** 013022
[30] Xu C, Feng J, Xiang H, and Bellaiche L 2018 *npj Comput. Mater.* **4** 57
[31] Xu C, Feng J, Kawamura M, Yamaji Y, Nahas Y, Prokhorenko S, Qi Y, Xiang H, and Bellaiche L 2020 *Phys. Rev. Lett.* **124** 087205
[32] Stavropoulos P P, Liu X, and Kee H Y 2021 *Phys. Rev. Res.* **3** 013216
[33] Maksimov P A and Chernyshev A L 2020 *Phys. Rev. Res.* **2** 033011
[34] Luo Q, Zhao J, Kee H Y, and Wang X 2021 *npj Quantum Mater.* **6** 57
[35] Luo Q, Zhao J, Li J, and Wang X 2024 *Phys. Rev. B* **110** 035121
[36] Luo Q, Stavropoulos P P, Gordon J S, and Kee H Y 2022 *Phys. Rev. Res.* **4** 013062
[37] Luo Q and Kee H Y 2022 *Phys. Rev. B* **105** 174435
[38] Luo Q, Zhao J, Wang X, and Kee H Y 2021 *Phys. Rev. B* **103** 144423
[39] Luo Q, Hu S, and Kee H Y 2021 *Phys. Rev. Res.* **3** 033048
[40] Luo Q, Hu S, Li J, Zhao J, Kee H Y, and Wang X 2023 *Phys. Rev. B* **107** 245131
[41] Rau J G, Lee E K H, and Kee H Y 2014 *Phys. Rev. Lett.* **112** 077204
[42] Kitagawa K, Takayama T, Matsumoto Y, Kato A, Takano R, Kishimoto Y, Bette S, Dinnebier R, Jackeli G, and Takagi H 2018 *Nature* **554** 341
[43] Bahrami F, Lafargue-Dit-Hauret W, Lebedev O I, Movshovich R, Yang H Y, Broido D, Rocquefelte X, and Tafti F 2019 *Phys. Rev. Lett.* **123** 237203
[44] Banerjee A, Bridges C A, Yan J Q *et al.* 2016 *Nat. Mater.* **15** 733
[45] Sears J A, Zhao Y, Xu Z, Lynn J W, and Kim Y J 2017 *Phys. Rev. B* **95** 180411

[46] Baek S H, Do S H, Choi K Y, Kwon Y S, Wolter A U B, Nishimoto S, van den Brink J, and Büchner B 2017 *Phys. Rev. Lett.* **119** 037201

[47] Wolter A U B, Corredor L T, Janssen L, Nenkov K, Schönecker S, Do S H, Choi K Y, Albrecht R, Hunger J, Doert T, Vojta M, and Büchner B 2017 *Phys. Rev. B* **96** 041405

[48] Wang Z, Reschke S, Hüvonen D, Do S H, Choi K Y, Gensch M, Nagel U, Rõõm T, and Loidl A 2017 *Phys. Rev. Lett.* **119** 227202

[49] Zheng J, Ran K, Li T, Wang J, Wang P, Liu B, Liu Z X, Normand B, Wen J, and Yu W 2017 *Phys. Rev. Lett.* **119** 227208

[50] Do S H, Park S Y, Yoshitake J, Nasu J, Motome Y, Kwon Y S, Adroja D T, Voneshen D J, Kim K, Jang T H, Park J H, Choi K Y, and Ji S 2017 *Nat. Phys.* **13** 1079

[51] Ran K, Wang J, Wang W, Dong Z Y, Ren X, Bao S, Li S, Ma Z, Gan Y, Zhang Y, Park J T, Deng G, Danilkin S, Yu S L, Li J X, and Wen J 2017 *Phys. Rev. Lett.* **118** 107203

[52] Winter S M, Riedl K, Maksimov P A, Chernyshev A L, Honecker A, and Valentí R 2018 *Nat. Commun.* **8** 1152

[53] Ran K, Wang J, Bao S, Cai Z, Shangguan Y, Ma Z, Wang W, Dong Z Y, Čermák P, Schneidewind A, Meng S, Lu Z, Yu S L, Li J X, and Wen J 2022 *Chin. Phys. Lett.* **39** 027501

[54] Panigrahi A, Coleman P, and Tsvelik A 2023 *Phys. Rev. B* **108** 045151

[55] Nasu J, Udagawa M, and Motome Y 2015 *Phys. Rev. B* **92** 115122

[56] Rousochatzakis I, and Perkins N B 2017 *Phys. Rev. Lett.* **118** 147204

[57] Chen K, Luo Q, Zhou Z, He S, Xi B, Jia C, Luo H G, and Zhao J 2023 *New J. Phys.* **25** 023006

[58] Rayyan A, Luo Q, and Kee H Y 2021 *Phys. Rev. B* **104** 094431

[59] Liu K, Sadoune N, Rao N, Greitemann J, and Pollet L 2021 *Phys. Rev. Res.* **3** 023016

[60] Saha P, Fan Z, Zhang D, and Chern G W 2019 *Phys. Rev. Lett.* **122** 257204

[61] Catuneanu A, Yamaji Y, Wachtel G, Kim Y B, and Kee H Y 2018 *npj Quantum Mater.* **3** 23

[62] Gohlke M, Wachtel G, Yamaji Y, Pollmann F, and Kim Y B 2018 *Phys. Rev. B* **97** 075126

[63] Gohlke M, Chern L E, Kee H Y, and Kim Y B 2020 *Phys. Rev. Res.* **2** 043023

[64] Wang J, Normand B, and Liu Z X 2019 *Phys. Rev. Lett.* **123** 197201

[65] Buessen F L and Kim Y B 2021 *Phys. Rev. B* **103** 184407

[66] Wang W, Dong Z Y, Yu S L, and Li J X 2017 *Phys. Rev. B* **96** 115103

[67] Stavropoulos P P, Catuneanu A, and Kee H Y 2018 *Phys. Rev. B* **98** 104401

[68] Chaloupka J and Khaliullin G 2015 *Phys. Rev. B* **92** 024413

[69] Li X, Zhao J, Li J, and Luo Q 2025 *Phys. Rev. B* **111** 064416

[70] Yang W, Nocera A, Tummuru T, Kee H Y, and Affleck I 2020 *Phys. Rev. Lett.* **124** 147205

[71] Yang W, Nocera A, Sørensen E S, Kee H Y, and Affleck I 2021 *Phys. Rev. B* **103** 054437

[72] Zhu Z, Kimchi I, Sheng D N, and Fu L 2018 *Phys. Rev. B* **97** 241110

[73] Hickey C and Trebst S 2019 *Nat. Commun.* **10** 530

[74] Patel N D and Trivedi N 2019 *Proc. Natl. Acad. Sci. USA* **116** 12199

[75] Jiang M H, Liang S, Chen W, Qi Y, Li J X, and Wang Q H 2020 *Phys. Rev. Lett.* **125** 177203

[76] Zhang S S, Halász G B, and Batista C D 2022 *Nat. Commun.* **13** 399

[77] Wang K, Feng S, Zhu P, Chi R, Liao H J, Trivedi N, and Xiang T 2024 arXiv:2403.12141 [cond-mat.str-el]

[78] Koga A, Tomishige H, and Nasu J 2018 *J. Phys. Soc. Jpn.* **87** 063703

[79] Oitmaa J, Koga A, and Singh R R P 2018 *Phys. Rev. B* **98** 214404

[80] Lee H Y, Kawashima N, and Kim Y B 2020 *Phys. Rev. Res.* **2** 033318

[81] Chen Y H, Genzor J, Kim Y B, and Kao Y J 2022 *Phys. Rev. B* **105** L060403

[82] Zhu Z, Weng Z Y, and Sheng D N 2020 *Phys. Rev. Res.* **2** 022047

[83] Hickey C, Berke C, Stavropoulos P P, Kee H Y, and Trebst S 2020 *Phys. Rev. Res.* **2** 023361

[84] Khait I, Stavropoulos P P, Kee H Y, and Kim Y B 2021 *Phys. Rev. Res.* **3** 013160